Solution equilibria and antitumor activity of pentamethylcyclopentadienyl rhodium complexes of picolinic acid and deferiprone

ÉVA A. ENYEDY[a*], ORSOLYA DÖMÖTÖR[a,b], CARMEN M. HACKL[c], ALEXANDER ROLLER[c], MARIA S. NOVAK[c], MICHAEL A. JAKUPEC[c,d], BERNHARD K. KEPPLER[c,d], WOLFGANG KANDIOLLER[c,d]

[a] Department of Inorganic and Analytical Chemistry, University of Szeged, Dóm tér 7, H-6720 Szeged, Hungary

[b] MTA-SZTE Bioinorganic Chemistry Research Group, University of Szeged, Dóm tér 7, H-6720 Szeged, Hungary

[c] Institute of Inorganic Chemistry, University of Vienna, Waehringer Str. 42, A-1090 Vienna, Austria

[d] University of Vienna, Research Platform "Translational Cancer Therapy Research", Waehringer Str. 42, A-1090 Vienna, Austria

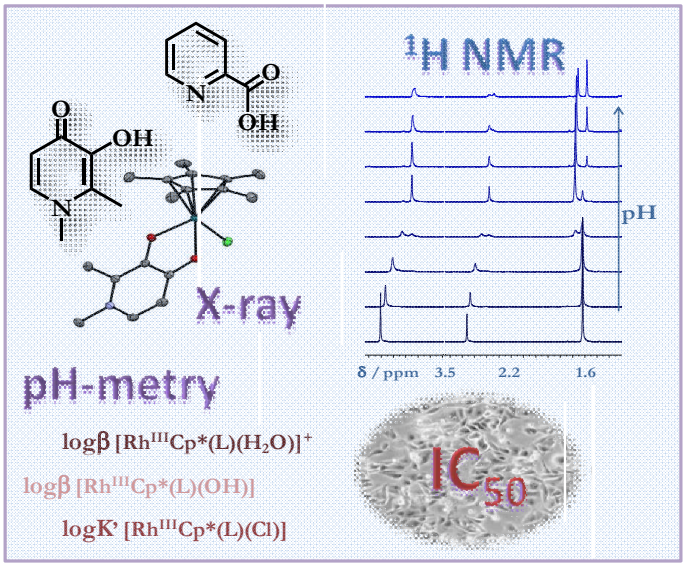

Keywords: Stability Constants; Cytotoxicity; Aquation; Synthesis; Crystal structure

*Corresponding author. E-mail: enyedy@chem.u-szeged.hu

Abstract Complex formation processes of rhodium(III)-η^5-pentamethylcyclopentadienyl cation $[RhCp^*(H_2O)_3]^{2+}$ with 1,2-dimethyl-3-hydroxy-pyridin-4(1H)-one (deferiprone, dhp) and pyridine-2-carboxylic acid (pic) were studied with the aid of pH-potentiometry, ^{1}H NMR and UV-visible spectrophotometry in aqueous solution in the presence and in the absence of chloride ions. Stoichiometry and overall stability constants of the complexes formed were determined. Formation of mononuclear, mono-ligand complexes such as [RhCp*(L)Z] (where L = dhp or pic; Z = Cl^- or H_2O) and mixed-hydroxido species [RhCp*(L)(OH)] was found. Relatively high pK_a values (9.32−11.90) were determined for the hydrolysis of the [RhCp*(L)Z] complexes. [RhCp*(L)Z] species predominate at physiological pH, and negligible decomposition is probable only at low micromolar concentrations. More favored complex formation was found in the case of pic. Stability of the studied organorhodium complexes was compared to analogous Ru(II)(η^6-*p*-cymene) compounds. In addition, the aqua/chlorido ligand replacement reaction in the complexes $[RhCp^*(L)(H_2O)]^+$ of dhp and pic was monitored to provide equilibrium constants with which the extent of aquation at various chloride concentrations can be estimated. Single crystals of [RhCp*(dhp)Cl] suitable for X-ray diffraction analysis were also obtained. The [RhCp*(L)Cl] complexes of dhp and pic were tested for cytotoxicity in various human cancer cell lines where they showed activity depending on the attached ligand scaffold.

1. Introduction

The research area of metal-based anticancer drugs was mainly fueled by the groundbreaking development of cisplatin (*cis*-diamminedichloridoplatinum(II)), one of the leading agents in clinical use. Despite the importance and pharmacological activity of Pt drugs, especially in combination therapy, there are exciting efforts to develop novel types of antitumor agents seeking to overcome intrinsic and acquired resistance phenomena and side effects of these Pt containing drugs [1-3]. The novel drug candidates need to exhibit improved efficacy and selectivity as well as more tolerable side effects as compared to established chemotherapeutics. Complexes of the neighboring transition metals such as Ru, Os, Ir and Rh are an attractive alternative field of drug development beside the platinum area. Ru(III)-based complexes such as *trans*-[tetrachlorido(1H-imidazole)(dimethylsulfoxide-κ*S*)ruthenate(III)] (NAMI-A) [4] and indazolium *trans*-[tetrachloridobis(1H-indazole)ruthenate(III)] (KP1019) [5] are the best studied representatives, and the sodium analogue KP1339 [6] of the latter is currently investigated in clinical trials. Organometallic "piano stool" η^6-arene (such as *p*-cymene, biphenyl, tetrahydroanthracene) or η^5-cyclopentadienyl water-soluble complexes of Ru and Os are extensively investigated, and some of them are active against tumor cells which have become resistant to cisplatin [7,8]. However, relatively few studies are focused on related Rh(II/III) compounds with antitumor activity [9-11]. The anticancer properties of $RhCl_3$ and its simple complexes such as *mer*-$[RhCl_3(NH_3)_3]$ were already reported some decades ago [12,13]. Effective inhibition of the viability of human cancer cells was found in the case of various dirhodium(II,II) carboxylate complexes [14,15]. Promising antiproliferative activities measured in human cancer cell lines have been reported for half-sandwich Rh complexes of bidentate polypyridyl ligands by Sheldrick *et al.* [16-18].

In the half-sandwich complexes of Rh(III) the ligand exchange processes are considerably faster compared to the hexaaqua complex, especially when anionic ligands (such as pentamethylcyclopentadienyl) are coordinated [9]. Additionally, the type of the co-ligand(s) has strong effect on physical-chemical and biological properties of the organometallic complex such as the solution stability and the hydro-lipophilic character, which can influence cellular uptake, pharmacokinetics and biological activity. Knowledge of the thermodynamics and kinetics of aquation (or designated as hydrolysis, *i.e.* replacement of the leaving group by a water molecule), ligand substitution (*i.e.* replacement of the co-ligand by water molecules or endogenous compounds) is a mandatory prerequisite for understanding

the transformation processes of the metallodrugs in the aqueous phase under physiological conditions and their mechanism of action [8,19].

Recently, we reported Rh(III)-η^5-pentamethylcyclopentadienyl (RhCp*) complexes bearing 3-hydroxyflavone and 3-hydroxy-4-pyrone ligands [20,21]. These 3-hydroxyflavone complexes have very limited water solubility, and their cytotoxicity could not be tested [20]. Complexes of 3-hydroxy-2-methyl-pyran-4(1H)-one (maltol) and 5-hydroxy-2-methyl-pyran-4(1H)-one (allomaltol) with much better solubility were tested in the human cancer cell lines CH1, SW480 and A549 and were found to exhibit minor cytotoxicity with IC_{50} values of ~100–300 μM [21]. Detailed solution equilibrium studies of RhCp* complexes formed with various ligands are fairly rare in the literature [22-24], especially which provide stability constants. Our previous work on RhCp* complexes of maltol and allomaltol revealed the formation of mono-ligand species which predominate at physiological pH and can decompose partially at micromolar concentrations on the basis of the determined stability constants [21]. In this work our aim was to investigate the effect of the exchange of the (O,O) donor hydroxypyrone ligands for a hydroxypyridinone or an (N,O) donor (picolinate) on the stability and the biological activity. For these studies, the well-known hydroxypyridinone, 1,2-dimethyl-3-hydroxy-pyridin-4(1H)-one (deferiprone, dhp) and pyridine-2-carboxylic acid (picolinic acid, pic) (see chart 1) were chosen. Analogous Ru(II)(η^6-*p*-cymene) and Os(II)(η^6-*p*-cymene) complexes of pic have been reported to show moderate antiproliferative activity [8,25], although the IrCp* complex of pic represents quite low efficacy [26].

Chart 1

Here we report the solution equilibria of RhCp* complexes of dhp and pic studied by pH-potentiometry, ^{1}H NMR spectroscopy and UV-visible (UV-Vis) spectrophotometry. The chlorido/aqua co-ligand exchange processes in the complex [RhCp*(L)Cl] (where L = dhp or pic) of the chosen ligands was also monitored. Stability constants of the complexes were determined in the presence and in the absence of the competitive chloride ions. Additionally, the [RhCp*(L)Cl] complexes of dhp and pic were synthesized (see chart 2), and their biological activity was investigated in human cancer cells.

Chart 2

2. Experimental section

2.1. Chemicals

All solvents were of analytical grade and used without further purification. Dhp, pic, sodium methoxide, KCl, KNO_3, $AgNO_3$, HCl, HNO_3 and KOH were purchased from Sigma-Aldrich and used without further purification. Dimeric rhodium precursor $[RhCp^*(\mu\text{-}Cl)Cl]_2$ and chlorido[1,2-dimethyl-3-(oxo-κO)-pyridin-4(1H)-onato-κO](η^5-1,2,3,4,5-pentamethylcyclopentadienyl)rhodium(III) (**1**) and chlorido[2-pyridine-2-carboxylato](η^5-1,2,3,4,5-pentamethylcyclopentadienyl)rhodium(III) (**2**) were prepared according to literature procedures [27,28]. Elemental analyses were carried out with a Perkin Elmer 2400 CHN Elemental Analyzer by the Microanalytical Laboratory of the University of Vienna. NMR spectra were recorded at 25 °C using a Bruker FT-NMR spectrometer Avance III^{TM} 500 MHz. ^{1}H-NMR spectra were measured at 500.10 MHz and ^{13}C{1H}-NMR spectra at 125.75 MHz in d_4-MeOH. The 2D NMR spectra were measured in a gradient-enhanced mode. The exact concentration of the ligand stock solutions together with the proton dissociation constants were determined by pH-potentiometric titrations with the help of the computer program HYPERQUAD [29]. A stock solution of $[RhCp^*Z_3]$ (where Z = H_2O and/or Cl^-; charges are omitted for simplicity) was obtained by dissolving a known amount of $[RhCp^*(\mu\text{-}Cl)Cl]_2$ in water, while the stock solution of $[RhCp^*(H_2O)_3](NO_3)_2$ was obtained from an aqueous solution of $[RhCp^*(\mu\text{-}Cl)Cl]_2$ after removal of chloride ions using equivalent amounts of $AgNO_3$. The exact concentrations of the RhCp* stock solutions (with or without chloride) were checked by pH-potentiometric titrations employing our previously published stability constants for $[(RhCp^*)_2(hydroxido)_i]$ (i = 2 or 3) complexes [21].

2.2. pH-Potentiometric measurements

The pH-potentiometric measurements for determination of the proton dissociation constants of the ligands and the overall stability constants of the RhCp* complexes were carried out at 25.0 ± 0.1 °C in water and at an ionic strength of 0.20 M KCl or KNO_3 used for keeping the activity coefficients constant. The titrations were performed with carbonate-free KOH solution (0.20 M). The exact concentrations of HCl, HNO_3 and KOH solutions were determined by pH-potentiometric titrations. An Orion 710A pH-meter equipped with a Metrohm combined electrode (type 6.0234.100) and a Metrohm 665 Dosimat burette were used for the pH-potentiometric measurements. The electrode system was calibrated to the pH = $-\log[H^+]$ scale by means of blank titrations (strong acid *vs.* strong base: HCl or HNO_3 *vs.*

KOH), as suggested by Irving *et al.* [30]. The average water ionization constant, pK_w, was determined as 13.76 ± 0.01 at 25.0 °C, I = 0.20 M (KCl, KNO_3), which corresponds well to the literature [31]. The reproducibility of the titration points included in the calculations was within 0.005 pH units. The pH-potentiometric titrations were performed in the pH range 2.0−11.5. The initial volume of the samples was 10.0 mL. The ligand concentration was 1.0−2.0 mM and metal ion-to-ligand ratios of 1:1 to 1:4 were used. The accepted fitting of the titration curves was always less than 10 μL. Samples were degassed by bubbling purified argon through them for *ca.* 10 min prior to the measurements and it was also passed over the solutions during the titrations.

The computer program PSEQUAD [32] was utilized to establish the stoichiometry of the complexes and to calculate the overall stability constants. $\beta(M_pL_qH_r)$ is defined for the general equilibrium (1):

$$pM + qL + rH \rightleftharpoons M_pL_qH_r \text{ as } \beta(M_pL_qH_r) = [M_pL_qH_r]/[M]^p[L]^q[H]^r \quad (1)$$

where M denotes the metal moiety RhCp* and L the completely deprotonated ligand. Literature logβ values of the various RhCp* - hydroxido complexes formed in the absence and presence of chloride ions were used [21] and compared to data collected in the course of the experiments described herein. In all calculations exclusively titration data were used from experiments in which no precipitate was visible in the reaction mixture.

2.3. UV–Vis spectrophotometric and ^{1}H NMR measurements

A Hewlett Packard 8452A diode array spectrophotometer was used to record the UV-Vis spectra in the interval 200–800 nm. The path length was 1 cm. UV–Vis measurements for [RhCp*Z_3] – pic system were carried out at 1:1 metal-to-ligand ratio by preparing individual samples in which KCl or KNO_3 was partially or completely replaced by HCl or HNO_3 and pH values, varying in the range *ca.* 0.7–2.0, were calculated from the strong acid content. The H_2O/Cl^- exchange processes in the complexes [RhCp*(L)(H_2O)] (where L = dhp or pic) were followed spectrophotomerically ($c_{complex}$ = 270 μM) at pH 7.40 (L = dhp) or at pH 3.50 (L = pic) while the Cl^- concentration was varied between 0 and 1.0 M. Stability constants of the complexes [RhCp*(pic)Z] and logK' for the H_2O/Cl^- exchange process were calculated with the computer program PSEQUAD [32].

^{1}H NMR titrations were carried out on a Bruker Ultrashield 500 Plus instrument. All spectra were recorded with the WATERGATE water suppression pulse scheme using 4,4-

dimethyl-4-silapentane-1-sulfonic acid as an internal NMR standard. The ligands were dissolved in a 10% (v/v) D_2O/H_2O mixture to yield a concentration of 1 mM and were titrated at 25 °C, at I = 0.20 M (KCl or KNO_3) in absence or presence of [RhCp*Z_3] at 1:1 metal-to-ligand ratio.

2.4. Synthesis of RhCp* complexes of dhp and pic

Chlorido[1,2-dimethyl-3-(oxo-κO)-pyridin-4(1H)-onato-κO](η^5-1,2,3,4,5-pentamethylcyclopentadienyl)rhodium(III) **1**

Standard procedure: dhp (100 mg, 0.72 mmol, 1 eq) and sodium methoxide (43 mg, 0.79 mmol, 1.1 eq) were dissolved in dry methanol (20 mL) and [RhCp*(μ-Cl)Cl]$_2$ (200 mg, 0.32 mmol, 0.9 eq) was added in one portion. The obtained deep red solution was stirred for 26 h at room temperature. The solvent was removed under reduced pressure; the residue was dissolved in CH_2Cl_2, filtered, concentrated and precipitated with diethyl ether. The red product was separated by filtration and dried *in vacuo* (153 mg, 57%). The isolated yield was found to be lower compared to the literature data (90%) [28]. ^{1}H NMR (500.10 MHz, $CDCl_3$): δ = 1.72 (s, 15H, -$CH_{3,Cp*}$), 2.40 (s, 3H, 2-$CH_{3,Pyr}$), 3.59 (s, 3H, N-CH_3), 6.34 (d, ^3J(H,H) = 7 Hz, 1H, H5), 6.90 (d, ^3J(H,H) = 7 Hz, 1H, H6); ^{13}C NMR (125.75 MHz, $CDCl_3$): δ = 8.8 (-$CH_{3,Cp*}$), 12.3 (-$CH_{3,C1}$), 40.3 (N-CH_3), 90.6 (C_{Cp*}), 109.7 (C5), 131.6 (C6), 132.3 (C2), 161.3 (C3), 175.6 (C4); Elemental analysis calcd (%) for $C_{17}H_{23}ClNO_2Rh$*0.75H_2O: C 48.02, H 5.81, N 3.29; found: C 48.04, H 5.74, N 3.22.

Chlorido[2-pyridine-2-carboxylato](η^5-1,2,3,4,5-pentamethylcyclopentadienyl)rhodium(III) **2**

Standard procedure: pic (91 mg, 0.72 mmol, 1 eq) and sodium methoxide (43 mg, 0.79 mmol, 1.1 eq) were dissolved in dry methanol (20 mL) and [RhCp*(μ-Cl)Cl]$_2$ (200 mg, 0.32 mmol, 0.9 eq) was added in one portion. The obtained orange solution was stirred for 18 h at room temperature. The solvent was removed under reduced pressure; the residue was dissolved in CH_2Cl_2, filtered, concentrated and precipitated with diethyl ether. The orange product was separated by filtration and dried *in vacuo* (180 mg, 70%). The yield was found to be lower compared to the literature data (81%) [28]. ^{1}H NMR (500.10 MHz, $CDCl_3$): δ = 1.77 (s, 15H, -$CH_{3,Cp*}$), 7.58–7.65 (m, 1H, H5), 7.97–8.00 (m, 1H, H4), 8.16 (d, ^3J(H,H) = 8 Hz, 1H, H3), 8.60 (d, ^3J(H,H) = 5 Hz, 1H, H6); ^{13}C NMR (125.75 MHz, $CDCl_3$): δ = 9.0 (-$CH_{3,Cp*}$), 93.9 (C_{Cp*}), 127.2 (C3), 128.0 (C5), 139.3 (C4), 149.0 (C2), 153.0 (C6), 170.0

(COO^-); Elemental analysis calcd (%) for $C_{16}H_{19}ClO_2NRh*0.5H_2O$: C 47.49, H 4.98, N 3.46; found: C 47.74, H 4.94, N 3.41.

2.5. Crystallographic structure determination

Single crystals of **1** were obtained by using the slow diffusion method from $CHCl_3$/*n*-hexane and analyzed on a Bruker D8 Venture diffractometer at 100 K. The single crystal was positioned at 35 mm from the detector and 2243 frames for 6.4 s exposure time over 0.4° scan width were measured. The data were processed using the SAINT software package [33]. The structures were solved by direct methods and refined by full-matrix least-squares techniques. Non-hydrogen atoms were refined with anisotropic displacement parameters. Hydrogen atoms were inserted at calculated positions and refined with a riding model. The following computer programs were used: structure solution, SHELXS-97 [34]; refinement, SHELXL-2013 [34]; OLEX2 [35]; SHELXLE [36]; molecular diagrams, ORTEP-3 [37]; scattering factors [38]. The crystallographic data files for **1** have been deposited with the Cambridge Crystallographic Database as CCDC 1024661.

2.6. Cell lines and culture conditions, cytotoxicity tests in cancer cell lines

Cell lines and culture conditions: CH1 cells originate from an ascites sample of a patient with an adenocarcinoma of the ovary and were a gift from Lloyd R. Kelland, CRC Centre for Cancer Therapeutics, Institute of Cancer Research, Sutton, UK. SW480 (human adenocarcinoma of the colon) and A549 (human non-small cell lung cancer) cells were provided by Brigitte Marian (Institute of Cancer Research, Department of Medicine I, Medical University of Vienna, Austria). All cell culture reagents were obtained from Sigma-Aldrich and plastic ware from Starlab (Germany). Cells were grown in 75 cm^2 culture flasks as adherent monolayer cultures in Minimum Essential Medium (MEM) supplemented with 10% heat-inactivated fetal calf serum, 1 mM sodium pyruvate, 4 mM L-glutamine and 1% non-essential amino acids (from 100× ready-to-use stock). Cultures were maintained at 37 °C in humidified atmosphere containing 95% air and 5% CO_2.

MTT assay: Cytotoxicity was determined by the colorimetric MTT [3-(4,5-dimethyl-2-thiazolyl)-2,5-diphenyl-2H-tetrazolium bromide] microculture assay. For this purpose, cells were harvested from culture flasks by trypsinisation and seeded in 100 µL/well aliquots into

96-well microculture plates. Cell densities of 1.0×10^3 cells/well (CH1), 2.0×10^3 cells/well (SW480) and 3.0×10^3 cells/well (A549) were chosen in order to ensure exponential growth of untreated controls throughout the experiment. Cells were allowed to settle and resume exponential growth in drug-free complete culture medium for 24 h. Stock solutions of the test compounds in dimethyl sulfoxide (DMSO) were diluted in complete culture medium and added to the plates (100 µL/well) where the maximum DMSO content did not exceed 0.5%. After 96 h of exposure, all media were replaced with 100 µL/well of MTT/RPMI1640 mixture (six parts of RPMI1640 medium supplemented with 10% heat-inactivated fetal bovine serum and 4 mM L-glutamine; one part of 5 mg/mL MTT reagent in phosphate-buffered saline). After incubation for 4 h, the supernatants were removed and the formazan crystals formed by viable cells were dissolved in 150 µL DMSO per well. Optical densities at 550 nm were measured with a microplate reader (BioTek ELx808) by using a reference wavelength of 690 nm to correct for unspecific absorption. The quantity of viable cells was expressed as percentage of untreated controls, and 50% inhibitory concentrations (IC_{50}) were calculated from concentration-effect curves by interpolation. Evaluation is based on means from three independent experiments, each comprising three replicates per concentration level.

3. Results and discussion

3.1. Synthesis of organometallic Rh(III) complexes and characterization

The Rh precursor $[RhCp^*(\mu\text{-}Cl)Cl]_2$ was synthesized according to literature procedures by reaction of $RhCl_3$ with pentamethylcyclopentadiene [27]. The RhCp* complexes of dhp and pic (see chart 2) were obtained according to the procedure described by Abbott *et al.* [28]. The ligands were deprotonated by sodium methoxide, followed by conversion with the Rh(III) dimer at room temperature, and pure compounds were isolated after work up. The isolated yields were found to be 57% and 70% for the complexes of dhp and pic, respectively. The organometallic Rh(III) complexes were characterized by NMR spectroscopy (^1H, ^{13}C) and elemental analysis. The recorded ^1H NMR spectra confirmed the coordination of the anionic ligand scaffolds to the organorhodium fragments. The α-proton next to the carbonyl group of the pyrone ring was shifted to higher fields upon coordination of the metal ion, whereas the signal assigned to the β-proton of the backbone was found slightly low-field shifted compared to the free ligands (see figures S1 and S2), which is comparable to the analogous Ru(II) complexes [39]. The dhp organometallic was found to possess a remarkable high solubility in

PBS (> 100 mM) in contrast to the pic derivative (~1 mM in 1% DMSO/PBS), and both complexes were sufficient stable in aqueous solution to perform biological experiments.

Single crystals of **1** were obtained by the slow diffusion method from $CHCl_3$/*n*-hexane and the result of the X-ray diffraction study is shown in figure 1. Crystal data, data collection parameters, and structure refinement details are given in table 1. Complex **1** crystallized in the monoclinic space group $P2_1/n$. The Rh(III) center exhibits a pseudo-octahedral geometry ("piano-stool"), and the Cp* moiety occupies facially three coordination sites, while the deprotonated dhp ligand binds in a bidentate manner via its (O,O) donor atoms (Rh–O1: 2.1318(11) Å, Rh–O2: 2.0726(10) Å) and the coordination sphere is completed with a chlorido ligand (Rh–Cl: 2.4361(4) Å). In addition, three molecules of chloroform per complex co-crystallized in the elemental unit, and each of them was found in close proximity to the hetero atoms around the Rh(III) center, with short contacts of the $CHCl_3$ hydrogen to the respective donor atom (2.1–2.5 Å). The coordination sphere leads to a chiral center at the rhodium atom and both enantiomers were found in the unit cell. The measured bond length and angles between the metal center and the donor atoms were found in the same range as reported for related structures [28].

Figure 1

Table 1

3.2. Proton dissociation processes of the ligands and hydrolysis of $[RhCp^*(H_2O)_3]^{2+}$

Proton dissociation equilibria of the studied ligands dhp and pic are well known in the literature [40-42], and pK_a values determined by pH-potentiometry (see table 2) are in reasonably good agreement with data reported under identical conditions as used in this study [43,44] with the exception of dhp (at I = 0.20 M (KNO_3)) where no data were available.

Table 2

According to literature data the aqua complex $[RhCp^*(H_2O)_3]^{2+}$ has a pseudooctahedral piano-stool type geometry, while its major hydrolysis product is a μ-hydroxido-bridged dinuclear species, $[(RhCp^*)_2(\mu\text{-}OH)_3]^+$ [22,45]. Both structures were proved by X-ray crystallography [22,45]. Recently, we have reported the hydrolytic behavior of the species $[RhCp^*(H_2O)_3]^{2+}$ at various ionic strengths such as 0.20 M KNO_3 and 0.20 M KCl [21]. The stoichiometry and overall stability constants of the dimer hydroxido complexes $[(RhCp^*)_2(\mu\text{-}OH)_3]^+$ and $[(RhCp^*)_2(\mu\text{-}OH)_2Z_2]$ (Z = H_2O or Cl^-, charges are omitted) were determined by pH-potentiometric and ^1H NMR titrations (see table 2), and these data were

used in this work for the calculations. The equilibrium states can be always reached quite fast in the pH range 2−11.5 in both media. It was also found that the chloride ions suppress the hydrolysis and shift the formation of the hydroxide-bridged dimers to the higher pH range, thus hydrolysis starts at pH > ~5 and pH > ~6 in the absence and in the presence of chloride ions, respectively [21]. It is noteworthy that the tendency of [RhCp*Z_3] to hydrolyze is undoubtedly weaker compared to the isoelectric species [Ru(II)(η^6-*p*-cymene)Z_3] [46].

3.3. Complex formation of [RhCp*Z_3] with dhp and pic in chloride-free and chloride-containing media

Solution equilibrium processes in the [RhCp*Z_3] − dhp and pic systems were investigated in aqueous solutions by the combined use of pH-potentiometric and ^{1}H NMR titrations in the absence and presence of 0.20 M chloride ions. The complex formation takes place quickly, the equilibrium states establish in both media within 10 minutes in the pH range studied (2-11.5). The stoichiometries and overall stability constants of the metal complexes furnishing the best fits to the experimental titration data are listed in table 2. Formation of only mono-ligand complexes such as [ML] (as [RhCp*(L)Z] (charges are omitted) and [$ML_{-1}H_{-1}$] (as [RhCp*$(L)H_{-1}$] = [RhCp*(L)(OH)], *vide infra*) was detected.

According to the pH-potentiometric titration curves the complex formation with dhp starts already at pH ~2 in the chloride-free medium, while only at pH > 3.7 in the presence of chloride ions. This is in good agreement with the pH-dependent ^{1}H NMR data (see representative spectra in figure 2 in the presence of chloride ions). Since slow ligand-exchange processes can be observed in the ^{1}H NMR spectra of the [RhCp*Z_3] – dhp system with respect to the NMR time scale ($t_{1/2}$(obs) > ~1 ms), peaks belonging to the protons of the free or bound ligand and to the bound or non-bound Cp* moiety can be detected separately. Formation of complex [RhCp*(L)Z] can be clearly seen in the acidic pH range, which predominates between pH 6.5 and 9. Additionally, two parallel processes take place at pH > 9.5: i) The upfield shift of the peaks belonging to [RhCp*(L)Z] indicates the formation of the hydrolysis product [RhCp*(L)(OH)]; their signals are not separated since species with the same metal-to-ligand ratio in different protonation states represent usually fast exchange processes. ii) Signals assigned to free ligand and to the non-bound metal moiety appear in the spectra owing to the partial decomposition of mono-ligand complex. The integrated peak areas of the methyl protons of Cp* were converted to molar fractions and plotted together

with the concentration distribution curves (see figure 3) calculated on the basis of the stability constants obtained by pH-potentiometry. Fairly good correlations between the data of both methods were observed. Quite similar speciation was found in the chloride-free medium (in table 2), although the overall stability constants of the mono-ligand complexes are higher and p*K* of [RhCp*(L)Z] is significantly lower compared to those obtained in the presence of chloride ions. This difference can be explained by the fact that chloride ions acting as competitive ligands can suppress the formation of the complexes. It is noteworthy that a similar tendency was reported for RhCp* complexes of maltol, allomaltol and for Ru(II)(η^6-*p*-cymene) complexes formed with various ligands [21,44,47].

Figures 2 and 3

In the species [RhCp*(dhp)Z] the ligand coordinates via the anionic bidentate (O,O)-donor set as it was shown for complex **1** (see figure 1) by X-ray crystallography. Notably, X-ray crystal structures of analogous Ru(II)(η^6-*p*-cymene) and Os(II)(η^6-*p*-cymene) complexes of dhp reveal quite similar geometry [48]. On the other hand the species of the general formula [RhCp*(L)H_{-1}] are considered as mixed hydroxido [RhCp*(L)(OH)] species formed by deprotonation of the coordinated water molecule or (partly) by the replacement of the chlorido ligand in chloride-containing medium.

^{1}H NMR spectra recorded for the [RhCp*Z_3] – pic system depicted in figure 4 and the pH-potentiometric titration curves indicate that the complex formation takes place already in the strongly acidic pH range in both media. (The fractions of the free ligand and metal ion are fairly low at pH ~2). Thus the stability constants of species [RhCp*(pic)Z] were determined by deconvolution of the UV–Vis spectra measured between pH 0.7 and 2.0 (in table 2). These spectra were recorded for individual samples in which the KCl (or KNO_3) was partially or completely replaced by HCl (or HNO_3) and the actual pH values were calculated based on the strong acid content, while the changes of the metal-to-ligand charge-transfer and ligand bands were followed. The complex [RhCp*(pic)Z] predominates in a wide pH range including physiological pH as the concentration distribution curves show in figure 5a. In order to represent the significantly high stability of this complex molar fraction was computed as a function of total concentrations at pH 7.4 (see figure 5.b). Negligible decomposition of species [RhCp*(pic)Z] can be predicted even in the low-micromolar concentration range in both studied media. In this complex coordination through (N,O) donor atoms of picolinate was reported by Abbott *et al.* [28]. The partial hydrolysis and decomposition of species [RhCp*(L)Z] take place in the basic pH range (see figure 5.a) as it was observed in the case of

dhp as well. The pK_a of the complex [RhCp*(pic)(H_2O)] is higher by more than one order of magnitude than that of the analogous Ir(III) complex [26]. In order to exclude the possibility of the monodentate coordination of a second ligand via the pyridine nitrogen besides the (N,O) binding mode, ^{1}H NMR spectra were recorded at various ligand excess (not shown). Peaks being assigned merely to the mono-ligand complex of pic and the free ligand were observed and there was no indication for the formation of bis-ligand complexes.

Figures 4 and 5

The leaving group Z in the third coordination site of complexes [RhCp*(L)Z] of dhp and pic is most probably a water molecule in the absence of chloride ions. However, it can be partially (or completely) displaced by a chlorido ligand or the aquation of the chlorido complex can undergo after dissolution. Aquation (hydrolysis) is considered as an important step of the mechanism of action as in the case of many transition metal anticancer complexes [49] such as cisplatin [50] or [Ru(II)(η^6-*p*-cymene)(L)Cl] compounds [51]. The H_2O/Cl^- exchange process was found to be fast (taking place within ~10 minutes) in the case of the RhCp* complexes of pic and dhp. Since the displacement of water by chloride results in characteristic spectral changes in the UV-Vis spectra, stepwise stability constants (log $K'(H_2O/Cl^-)$ in table 2) could be estimated for the following equilibrium with the deconvolution of the spectra (see figure 6 for the dhp complex).

$$[RhCp^*(L)(H_2O)]^+ + Cl^- \rightleftharpoons [RhCp^*(L)Cl)] + H_2O \qquad (2)$$

Measurements were performed at pH values where [RhCp*(L)Z] complexes predominate.

Figure 6

Based on the H_2O/Cl^- exchange constant of the complex [RhCp*(pic)Z] concentration distribution curves were calculated at various chloride concentrations (see figure 7). It is noteworthy that the equilibrium constant of the pic complex is more than one order of magnitude higher than that of dhp or other (O,O) donor ligands [21], which may have effect on the bioactivity. With the aid of the $K'(H_2O/Cl^-)$ exchange constants we can estimate the ratio of the aqua and the chlorinated complexes at chosen chloride concentrations. *E.g.* At 100 mM chloride concentration, which corresponds to the blood plasma, 38% of the dhp and 94% of the pic complexes are chlorinated. While at the chloride concentration of the cell nucleus (4 mM) only 3% and 36% of the complexes of dhp and pic are chlorinated, respectively. (Calculations were done at 50 μM concentration of the complexes.)

Figure 7

3.4. Comparison of stability of [RhCp*Z_3] and [Ru(II)(η^5-p-cymene)Z_3] complexes formed with dhp and pic

Our aim in this work was to investigate the differences in the solution speciation of [RhCp*Z_3] complexes formed with the (O,O) donor 3-hydroxy-4-pyridinone and the (O,N) donor picolinate ligand. The complex formation equilibrium, which is characterized by the overall stability constant (β), is superimposed by other accompanying equilibria such as the (de)protonation of the ligand and the hydrolysis of the metal ion. Therefore the overall stability constants cannot be compared directly in the case of different ligands and metal ions. Derived constants (log K*, in table 2) taken into consideration the different basicities of the ligands according to the following competition reaction can be used to compare the stabilities:

$$[RhCp^*Z_3] + HL \rightleftharpoons [RhCp^*(L)Z] + H^+ + 2\,Z \quad (Z = H_2O \text{ or } Cl^-) \qquad (3)$$

The higher derived constants imply more favored complex formation. Log K* values of pic are undoubtedly higher than those of dhp and higher chelate stability is found in the absence of the competitive chloride ions.

On the other hand not only the competition of the metal ion with protons for the ligand but that of the ligand with the hydroxide for the metal ion has to be taken into consideration, which becomes more pronounced at higher and higher pH values. Conditional stability constants or pM values can be computed at a fixed pH value or as a function of pH. To indicate the difference in the metal binding ability of dhp, pic and maltol for comparison towards RhCp* pM values were calculated at various pH values under the same conditions (see figure 8). pM values give the negative logarithm of the equilibrium concentrations of the non-bound metal ion ([RhCp*Z_3] and the μ-hydroxido dinuclear species) under the given conditions. Higher pM values indicate stronger chelating ability. The coordination of pic to RhCp* starts at more acidic pH values compared with the (O,O) ligands and the RhCp* binding ability of the ligands show the following order: maltol < dhp < pic.

Figure 8

Overall stability constants of the analogous complexes formed in the Ru(II)(η^6-*p*-cymene) – dhp / pic / maltol systems are also available in the literature [41,44]. Log β values of the Ru(II)(η^6-*p*-cymene) complexes formed with dhp and maltol are higher compared to those of RhCp* species, although the picolinate complexes show reverse tendency. The hydrolysis constants of compounds Ru(II)(η^6-*p*-cymene) and RhCp* are significantly different and this fact has to be taken into consideration when the stabilities are compared. For

a more adequate comparison distribution diagrams were computed for these systems at physiological pH under identical circumstances with the aid of the overall stability constants (see figure 9). Mono-ligand complexes (mainly [MLZ]) predominate at this pH in all cases, although their fractions show remarkable differences. The fractions of the metal complexes formed with dhp are higher than those of maltol as it was expected since the lesser strength of bidentate binding of hydroxypyrones was also found in the case of other metal ions [41,52]. It is noteworthy that the metal binding ability of dhp towards Ru(II)(η^6-*p*-cymene) is comparable with RhCp* at this particular pH, while complexation of maltol is somewhat more favored with RhCp*. On the other hand preference for the (N,O) coordination of pic to RhCp* is observed over the binding of the (O,O) donor ligand dhp, although the molar fraction of the mono-ligand complexes of dhp is higher in the case of Ru(II)(η^6-*p*-cymene) representing some alterations in the binding abilities of these organometallic compounds.

Figure 9

3.5. Cytotoxicity of RhCp* complexes of dhp and pic

In our previous work, RhCp* complexes formed with hydroxypyrone ligands such as maltol and allomaltol were investigated for their anticancer potential in various human cancer cell lines [21]. They were found to exhibit minor cytotoxicity, being effective only in a range similar to that of the analogous Ru(II)(η^6-*p*-cymene) complexes [53]. Within this work the impact of the coordination of the (O,O) donor ligand dhp and the (N,O) donor pic to RhCp* on cytotoxicity was investigated by means of the colorimetric MTT assay in the human cancer cell lines CH1 (ovarian carcinoma), SW480 (colon carcinoma) and A549 (non-small cell lung carcinoma). Cytotoxicity data for the related Ru(II)(η^6-*p*-cymene), Os(II)(η^6-*p*-cymene) and Ir(III)Cp* complexes formed with pic are available in the literature [8,25,26]. The Ru(II)(η^6-*p*-cymene) complex of pic exhibits IC_{50} values of 36–82 μM measured against human cancer cell lines such as cervix carcinoma and melanoma cells [25].The cytotoxicity of the Os(II)(η^6-*p*-cymene)-pic complex falls in the range of 17–45 μM tested in lung and ovarian cancer cells [8]. However, complex **2** was found to be poorly cytotoxic with IC_{50} values between *ca.* 250–350 μM in the cell lines investigated here. It is noteworthy that the analogous IrCp* complex also showed fairly high IC_{50} values (> 100 μM) [26]. In contrast, the dhp derivative **1** exhibited moderate activity. CH1 cells were found to be most sensitive followed by SW480 and A549 cells (see table 3).

Table 3

Both studied complexes were found to be fairly stable in aqueous solution at pH 7.4. Complex **2** has somewhat higher stability and possesses higher log $K'(H_2O/Cl^-)$ value compared to complex **1**, while the cytotoxicity of the latter is roughly 2–5 times higher. Results represent no direct relationship between stability and bioactivity, although the stronger affinity towards chloride ions at the third coordination position seems to be disadvantageous. The anticancer activity is influenced by many other parameters such as the lipophilicity, size and interaction with transfer and target macromolecules and these essential binding events are currently investigated in our laboratories.

4. Conclusions

The goal of the present study was to characterize and compare the solution speciation of RhCp* complexes of ligands dhp and pic together with the investigation of their bioactivity. Stoichiometry and stability of the complexes were determined *via* a combined approach using pH-potentiometry, ^{1}H NMR spectroscopy and UV-Vis spectrophotometry in the absence and presence of chloride ions. Exclusive formation of the mono-ligand complexes such as [RhCp*(L)Z] (L = dhp or pic, Z = H_2O or Cl^-) and [RhCp*(L)(OH)] was detected. Pic forms higher stability complexes with RhCp* compared to dhp, although the stability of the complexes formed with this ligand significantly exceeds that of hydroxypyrones such as maltol. [RhCp*(L)Z] complexes of pic and dhp are predominant at physiological pH even in the micromolar concentration range. Partial decomposition of these complexes to the biologically inactive dinuclear tri-hydroxido bridged species $[(RhCp^*)_2(\mu\text{-}OH)_3]^+$ and to the metal-free ligand is expected on the basis of the determined overall stability constants in the basic pH range (at pH > ~8−9 depending on the type of ligand and chloride ion concentration). Formation of mixed hydroxido complexes [RhCp*(L)(OH)] was observed and could be characterized by relatively high pK_a values (9.32−11.90). Chloride ions act as competitive ligands and are able to suppress the formation of RhCp* complexes to some extent. Aquation process of [RhCp*(L)Cl] complexes may play an important role in the mechanism of action of this type of organometallics, and the extent of the chloride/water exchange depends on the chloride concentrations of the biofluid and the exchange constant. Therefore, the co-ligand exchange equilibrium for the $[RhCp^*(L)(H_2O)]^+$ complexes of dhp and pic was studied by UV-Vis spectrophotometry. Based on the constants it can be predicted

that, *e.g.*, ~38% of the dhp complex exists as the chlorido complex at 0.1 M chloride concentration in human blood plasma, whereas the pic complex has a much stronger ability to retain the chloride at the third coordination site.

In order to investigate the *in vitro* cytotoxicity of the RhCp* complexes of dhp and pic, the compounds were synthesized and characterized. The cytotoxicity of these organometallics was studied in the human cancer cell lines (CH1, SW480 and A549). The pic complex showed no relevant cytotoxicity, whereas the organorhodium dhp analogue exhibited moderate cytotoxicity depending on the cell line. Thus, the dhp complex was found to be significantly more active than the pic derivative, although the latter is more stable in aqueous solution and has higher H_2O/Cl^- exchange constant for the species [RhCp*(L)Z]. These results confirm that the cytotoxicity depends on the attached ligand scaffold, and the bioactive ligand scaffold dhp seems to be beneficial with regard to the anticancer potential.

Acknowledgment

This work was supported by the Hungarian Research Foundation OTKA project PD103905.

Supplemental material

Supplemental material related to this article can be found online at…

References

[1] M.A. Jakupec, M. Galanski, V.B. Arion, C.G. Hartinger, B.K. Keppler, *Dalton Trans.,* 183 (2008).

[2] G.N. Kaluderovic, R. Paschke, *Curr. Med. Chem.,* **18**, 4738 (2011).

[3] Y. Jung, S.J. Lippard, *Chem. Rev.,* **107**, 1387 (2007).

[4] E. Alessio, G. Mestroni, A. Bergamo, G. Sava, *Curr. Top. Med. Chem.,* **4**, 1525 (2004).

[5] C.G. Hartinger, M.A. Jakupec, S. Zorbas-Seifried, M. Groessl, A. Egger, W. Berger, H. Zorbas, P.J. Dyson, B.K. Keppler, *Chem. Biodiversity,* **5**, 2140 (2008).

[6] P. Heffeter, K. Böck, B. Atil, M.A.R. Hoda, W. Körner, C. Bartel, U. Jungwirth, B.K. Keppler, M. Micksche, W. Berger, G. Koellensperger, *J. Biol. Inorg. Chem.,* **15**, 737 (2010).

[7] A.A. Nazarov, C.G. Hartinger, P.J. Dyson, *J. Organomet. Chem.,* **751**, 251 (2014).

[8] A.F.A. Peacock, S. Parsons, P.J. Sadler, *J. Am. Chem. Soc.,* **129**, 3348 (2007).

[9] Y. Geldmacher, M. Oleszak, W.S. Sheldrick, *Inorg. Chim. Acta,* **393**, 84 (2012).

[10] S. Top, I. Efremenko, M.N. Rager, A. Vessières, P. Yaswen, G. Jaouen, R.H. Fish, *Inorg. Chem.,* **50**, 271 (2011).

[11] C.H. Leung, H.J. Zhong, D.S.H. Chan, D.L. Ma, *Coord. Chem. Rev.,* **257**, 1764 (2013).

[12] A. Taylor, N. Carmichael, *Cancer Studies,* **2**, 36 (1953).

[13] M.J. Cleare, P.C. Hydes, *Met. Ions Biol. Syst.,* **11**, 1 (1980).

[14] S.U. Dunham, H.T. Chifotides, S. Mikulski, A.E. Burr, K.R. Dunbar, *Biochemistry,* **44**, 996 (2005).

[15] J.D. Aguirre, A.M. Angeles-Boza, A. Chouai, J.-P. Pellois, C. Turro, K.R. Dunbar, *J. Am. Chem. Soc.,* **131**, 11353 (2009).

[16] S. Schäfer, I. Ott, R. Gust, W.S. Sheldrick, *Eur. J. Inorg. Chem.,* **19**, 3034 (2007).

[17] M.A. Nazif, R. Rubbiani, H. Alborzinia, I. Kitanovic, S. Wolfl, I. Ott, W.S. Sheldrick, *Dalton Trans.,* **41**, 5587 (2012).

[18] Y. Geldmacher, K. Splith, I. Kitanovic, H. Alborzinia, S. Can, R. Rubbiani, M.A. Nazif, P. Wefelmeier, A. Prokop, I. Ott, S. Wölfl, I. Neundorf, W.S. Sheldrick, *J. Biol. Inorg. Chem.,* **17**, 631 (2012).

[19] T. Kiss, T. Jakusch, B. Gyurcsik, A. Lakatos, É.A. Enyedy, É. Sija, *Coord. Chem. Rev.,* **256**, 125 (2012).

[20] M.B. Schwarz, A. Kurzwernhart, A. Roller, W. Kandioller, B.K. Keppler, C.G. Hartinger, *Z. Anorg. Allg. Chem.,* **639**, 1648 (2013).

[21] O. Dömötör, S. Aicher, M. Schmidlehner, M.S. Novak, A. Roller, M.A. Jakupec, W. Kandioller, C.G. Hartinger, B.K. Keppler, É.A. Enyedy, *J. Inorg. Biochem.,* **134**, 57 (2014).

[22] M.S. Eisen, A. Haskel, H. Chen, M.M. Olmstead, D.P. Smith, M.F. Maestre, R.H. Fish, *Organometallics,* **14**, 2806 (1995).

[23] S. Ogo, H. Chen, M.M. Olmstead, R.H. Fish, *Organometallics,* **15**, 2009 (1996).

[24] D.P. Smith, H. Chen, Seiji Ogo, A.I. Elduque, M. Eisenstein, M.M. Olmstead, R.H. Fish, *Organometallics,* **33**, 2389 (2014).

[25] I. Ivanović, S. Grgurić-Šipka, Sanja; N. Gligorijević, S. Radulović, A. Roller, Z.L. Tešić, B.K. Keppler, *J. Serb. Chem. Soc.,* **76**, 53 (2011).

[26] Z. Liu, A. Habtemariam, A.M. Pizarro, S.A. Fletcher, A. Kisova, O. Vrana , L. Salassa, P.C.A. Bruijnincx, G.J. Clarkson, V. Brabec, P.J. Sadler, *J. Med. Chem.,* **54**, 3011 (2011).

[27] L. Booth, R.N. Haszeldine, M. Hill. *J. Chem. Soc. A,* 1299 (1969).

[28] A.P. Abbott, G. Capper, D.L. Davies, J. Fawcett, D.R.J. Russell, *J. Chem. Soc. Dalton Trans.,* 3709 (1995).

[29] P. Gans, A. Sabatini, A. Vacca, *Talanta,* **43**, 1739 (1996).

[30] H.M. Irving, M.G. Miles, L.D. Pettit, *Anal. Chim. Acta,* **38**, 475 (1967).

[31] SCQuery, The IUPAC Stability Constants Database, Academic Software (Version 5.5), Royal Society of Chemistry, (1993–2005).

[32] L. Zékány, I. Nagypál, in: *Computational Methods for the Determination of Stability Constants* (Ed.: D. L. Leggett), Plenum Press, New York, p. 291 (1985).

[33] M.R. Pressprich, J. Chambers, SAINT + Integration Engine, Program for Crystal Structure Integration, Bruker Analytical X-ray systems: Madison, (2004).

[34] G.M. Sheldrick, *Acta Cryst.,* **A64**, 112 (2008).

[35] O.V. Dolomanov, L.J. Bourhis, R.J. Gildea, J.A.K. Howard, H. Puschmann, *J. Appl. Cryst.,* **42**, 339 (2009).

[36] C.B. Hübschle, B. Dittrich, G.M. Sheldrick, *Acta Cryst.,* **A68**, 152 (2012).

[37] L.J. Farrugia, *J. Appl. Cryst.,* **30**, 565 (1997).

[38] *International Tables for X-ray Crystallography*. Kluwer Academic Press: Dordrecht, The Netherlands, **Vol. C.** , (1992).

[39] W. Kandioller, C.G. Hartinger, A.A. Nazarov, C. Bartel, M. Skocic, M.A. Jakupec, V.B. Arion, B.K. Keppler, *Chem. Eur. J.,* **15**, 12283 (2009).

[40] T. Jakusch, É.A. Enyedy, K. Kozma, Z. Paár, A. Bényei, T. Kiss, *Inorg. Chim. Acta,* **420**, 92 (2014).

[41] L. Bíró, E. Farkas, P. Buglyó, *Dalton Trans.,* **39**, 10272 (2010).

[42] E. Kiss, K. Petrohan, D. Sanna, E. Garribba, G. Micera, T. Kiss, *Polyhedron,* **19**, 55 (2000).

[43] É.A. Enyedy, L. Horváth, K. Gajda-Schrantz, G. Galbács, T. Kiss, *J. Inorg. Biochem.,* **100**, 1936 (2006).

[44] É. Sija, C.G. Hartinger, B.K. Keppler, T. Kiss, É.A. Enyedy, *Polyhedron,* **67**, 51 (2014).

[45] A. Nutton, P.M. Baily, P.M. Maitlis, *J. Chem. Soc. Dalton Trans.,* 1997 (1981).

[46] L. Bíró, E. Farkas, P. Buglyó, *Dalton Trans.,* **41**, 285 (2012).

[47] E.A. Enyedy, E. Sija, T. Jakusch, C.G. Hartinger, W. Kandioller, B.K. Keppler, T. Kiss, *J. Inorg. Biochem.,* **127**, 161 (2013).

[48] H. Henke, W. Kandioller, M. Hanif, B.K. Keppler, C.G. Hartinger, *Chem. Biodivers.,* **9**, 1718 (2012).

[49] A. M. Pizarro, A. Habtemariam, P.J. Sadler, In: *Medicinal Organometallic Chemistry* (Topics in Organometallic Chemistry), 1st ed., (Eds. G. Jaouen, N. Metzler-Nolte), Springer-Verlag: Heidelberg, Germany, **Vol. 32**, pp 21- 56. (2010).

[50] R.B. Martin, In: *Cisplatin: Chemistry and Biochemistry of a Leading Anticancer Drug*, (Ed. B. Lippert), VHCA & Wiley-VCH: Zürich, Switzerland, pp 181- 205 (1999).

[51] M. Melchart, A. Habtemariam, O. Novakova, S.A. Moggach, F.P.A. Fabbiani, S. Parsons, V. Brabec, P.J. Sadler, *Inorg. Chem.,* **46**, 8950 (2007).

[52] T. Kiss, T. Jakusch, D. Hollender, É.A. Enyedy, L. Horváth, *J. Inorg. Biochem.,* **103**, 527 (2009).

[53] W. Kandioller, A. Kurzwernhart, M. Hanif, S.M. Meier, H. Henke, B.K. Keppler, C.G. Hartinger, *J. Organomet. Chem.,* **696**, 999 (2011).

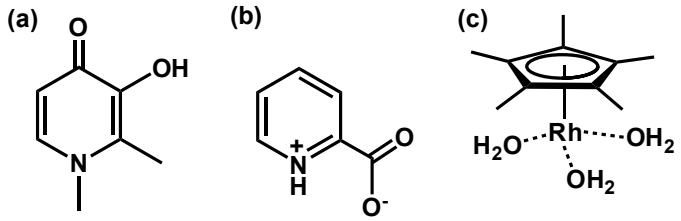

Chart 1. Chemical structures of dhp (a), pic (b) in their neutral forms and $[RhCp^*(H_2O)_3]^{2+}$ (c).

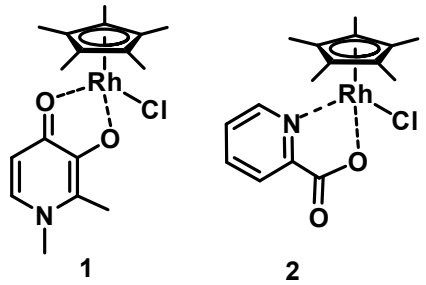

Chart 2. Chemical structures of RhCp* complexes of dhp (**1**) and pic (**2**).

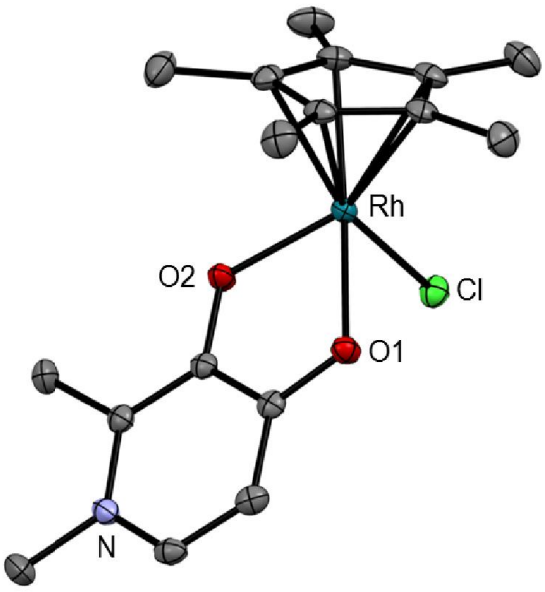

Figure 1. Solid state structure of complex **1** drawn at 50% probability level. Hydrogens and solvent molecules are omitted for clarity.

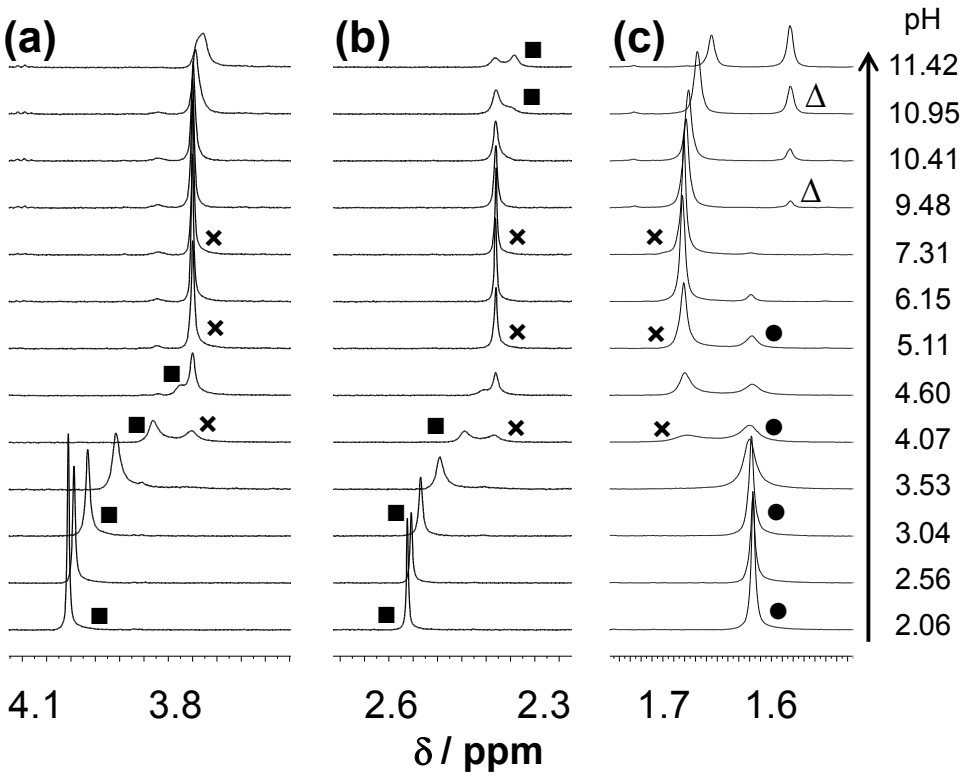

Figure 2. Representative ^{1}H NMR spectra of the [RhCp*Z_3] – dhp system in chloride-containing aqueous solution recorded at various pH values showing the regions of the chemical shifts of the methyl protons: N-CH_3 of dhp (a), C^2CH_3 of dhp (b) and CH_3 of Cp* (c). Symbols: ×: [RhCp*(dhp)Z], ■: free ligand (in different protonation states), ●: [RhCp*Z_3], Δ: $[(RhCp^*)_2(\mu\text{-}OH)_3]^+$. {$c_M = c_L = 1$ mM; T = 25 ˚C; I = 0.20 M (KCl); 10% D_2O; Z = H_2O or Cl^-}.

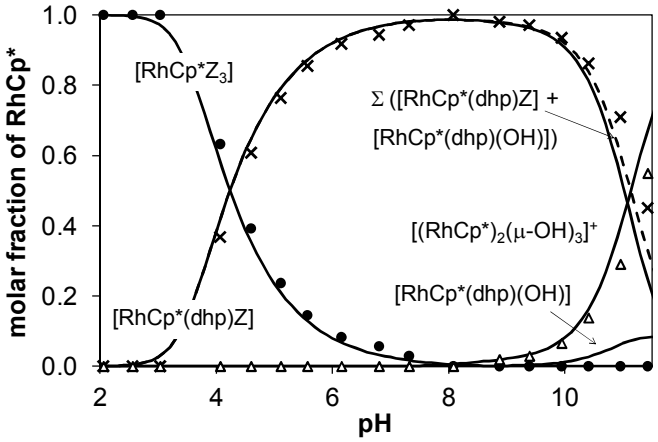

Figure 3. Concentration distribution curves of the $[RhCp^*Z_3]$ – dhp system calculated with the aid of the overall stability constants (solid lines). Molar fractions based on the ^1H NMR peak integrals of the methyl protons of Cp*. ×: [RhCp*(dhp)Z] and [RhCp*(dhp)(OH)] together; ●: $[RhCp^*Z_3]$; Δ: $[(RhCp^*)_2(\mu\text{-}OH)_3]^+$. {$c_M = c_L = 1$ mM; T = 25 ˚C; I = 0.20 M (KCl); 10% D_2O; Z = H_2O or Cl^-}.

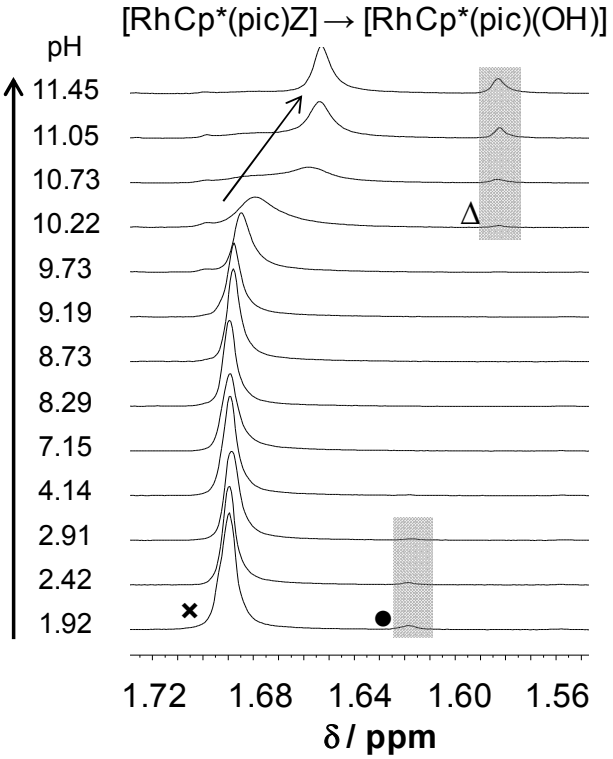

Figure 4. Representative ^1H NMR spectra of the $[RhCp^*Z_3]$ – pic system in chloride-containing aqueous solution recorded at various pH values showing the regions of the chemical shifts of the methyl protons of Cp*. Symbols: ×: [RhCp*(pic)Z]; ●: $[RhCp^*Z_3]$; Δ: $[(RhCp^*)_2(\mu\text{-}OH)_3]^+$. {$c_M = c_L =$ 1 mM; T = 25 ˚C; I = 0.20 M (KCl); 10% D_2O; Z = H_2O or Cl^-}.

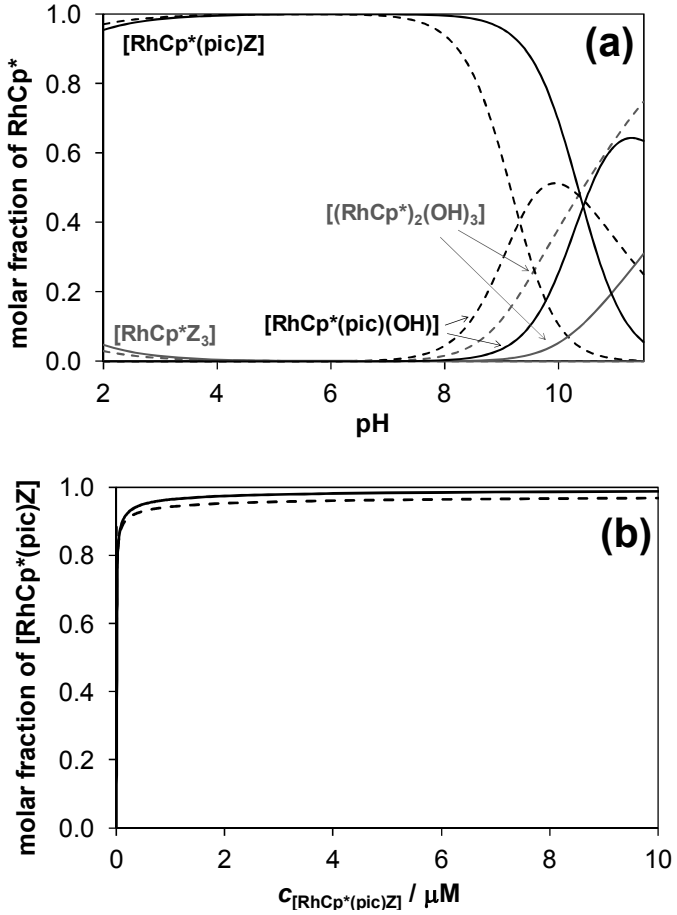

Figure 5. Concentration distribution curves of the [RhCp*Z_3] – pic (1:1) system in chloride-free (dotted lines) and chloride-containing (solid lines) aqueous solutions as a function of pH (a). Molar fractions of complex [RhCp*(pic)Z] plotted against analytical (total) complex concentrations at pH 7.40 in chloride-free (dotted lines) and chloride-containing (solid lines) solutions (b). {$c_M = c_L = 1$ mM (a); T = 25 ˚C; I = 0.20 M (KCl or KNO_3); Z = H_2O or Cl^-}.

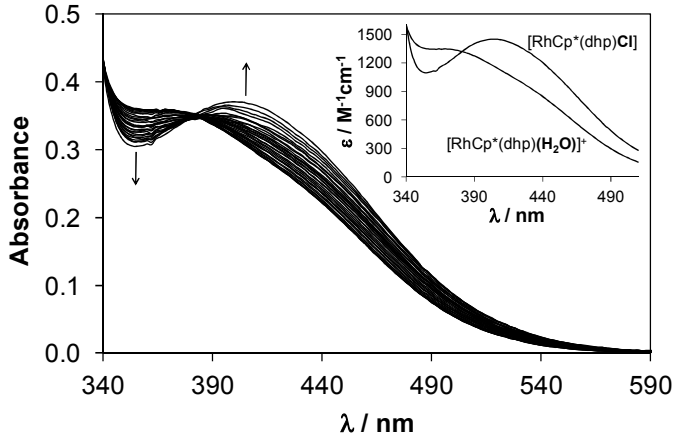

Figure 6. UV–Vis spectra recorded for the water/chloride exchange process in the complex [RhCp*(dhp)$(H_2O)]^+$ at physiological pH. Inset shows the individual calculated spectra of complexes [RhCp*(dhp)$(H_2O)]^+$ and [RhCp*(dhp)Cl]. {$c_M = c_L = 0.27$ mM; $c_{KCl} = 0–1.0$ M; T = 25 ˚C; pH = 7.40)}.

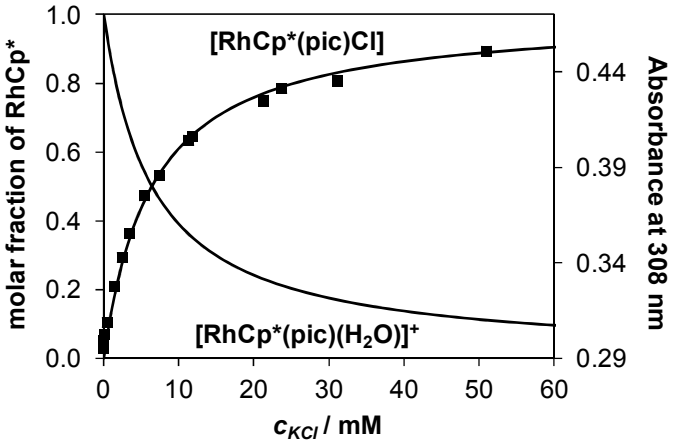

Figure 7. Absorbance values measured for the complex $[RhCp^*(pic)(H_2O)]^+$ at 308 nm (■) at various chloride ion concentrations and calculated concentration distribution curves (solid lines) calculated with the aid of the formation constant log *K' (H_2O/Cl^-)* for the water/chloride exchange process. {c_M = c_L = 0.27 mM; c_{KCl} = 0−51 mM; T = 25 ˚C; pH = 3.50}.

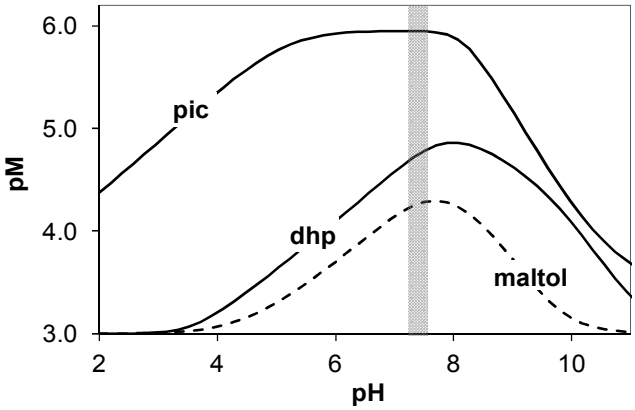

Figure 8. pH-dependence of pM values calculated for the $[RhCp^*Z_3]$ – pic / dhp / maltol systems under identical conditions. pM = –log[M]; where [M] is the equilibrium concentration of the ligand-free, non-bound metal ions. {c_M = 1 mM; M:L = 1:1; T = 25 ˚C; I = 0.20 M (KCl; Z = H_2O or Cl^-)} Calculation for the maltol-containing system is based on data from Ref. [21].

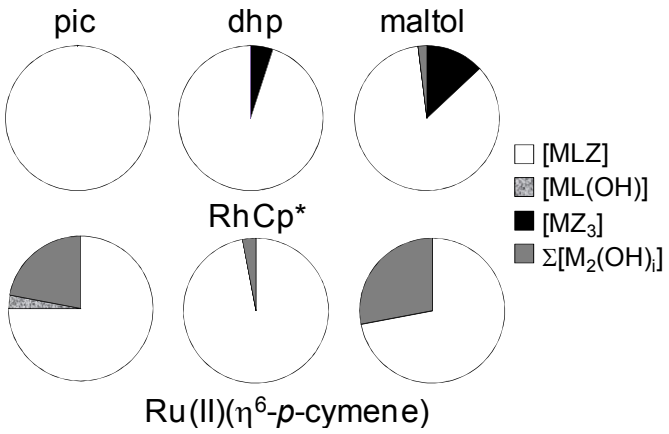

Figure 9. Concentration distribution diagrams of complexes formed in the [RhCp*Z_3] / [Ru(II)(η^6-*p*-cymene)Z_3] – dhp / pic / maltol systems calculated at physiological pH with the aid of the overall stability constants. {$c_M = c_L$ = 100 μM; pH = 7.40; T = 25 ˚C; I = 0.20 M (KCl; M = RhCp* or Ru(II)(η^6-p-cymene); Z = H_2O or Cl^-)} Calculations for the [RhCp*Z_3] – maltol and [Ru(II)(η^6-*p*-cymene)Z_3] containing systems are based on data from Refs. [21,41].

Table 1

Crystal data and details of data collection for the RhCp* complex of dhp (**1**)

Compound	**1**
Empirical formula	$C_{20}H_{23}ClNO_2Rh{\cdot}3CHCl_3$
Formula weight / g/mol	769.83
Temperature / K	100(0)
Wavelength /	0.71073
Crystal size / mm	0.12 × 0.15 × 0.30
Crystal system	monoclinic
space group	$P2_1/n$
a / Å	16.1522(10)
b / Å	9.5797(6)
c / Å	20.1702(16)
α / °	90.00
β/ °	108.2910(19)
γ / °	90.00
Volume / Å^3	2963.3(3)
Z	4
Calculated density / mg/m^3	1.726
Absorption coefficient / mm^{-1}	1.498
F(000)	1536
θ range for data collection	1.94–25.39°
Index ranges	-19 ≤ h ≤ 19
	-11≤ k ≤ 11
	-24 ≤ l ≤ 24
Reflections collected / unique	87951 / 5445
Data / restraints / parameters	5445 / 0 / 314
R(int)	0.0277
Goodness-of-fit on F^2 [a]	1.051
Final R indices [I>2σ(I)] [b]	
R_1	0.0182
wR_2	0.0449

[a] GOF = $\{\Sigma[w(F_o^2 - F_c^2)^2] /(n - p)\}^{1/2}$, where *n* is the number of reflections and *p* is the total number of parameters refined.

[b] $R_1 = \Sigma||F_o| - |F_c||/\Sigma|F_o|$. $wR_2 = \{\Sigma[w(F_o^2 - F_c^2)^2]/\Sigma[w(F_o^2)^2]\}^{1/2}$

Table 2

Proton dissociation constants (pK_a) of dhp and pic and overall stability constants (log β) of their RhCp* complexes in chloride-containing and chloride-free solutions determined by pH-potentiometry {T = 25 °C; I = 0.20 M}.[a]

	dhp		**pic**	
	0.20 M KCl	**0.20 M KNO_3**	**0.20 M KCl**	**0.20 M KNO_3**
pK_1 (ligand)	3.64 ± 0.01	3.67 ± 0.01	5.26 ± 0.01	5.21 ± 0.01
pK_2 (ligand)	9.77 ± 0.01	9.66 ± 0.01	–	–
log β [MLZ][b]	8.93 ± 0.01	10.90 ± 0.01	8.90 ± 0.01[c]	9.18 ± 0.01[c]
log β [MLH_{-1}][d]	−2.97 ± 0.07	0.23 ± 0.03	−1.54 ± 0.02	−0.14 ± 0.02
pK [MLZ]	11.90	10.67	10.44	9.32
log K* [e]	−0.84	+1.24	+3.64	+3.97
log K' (H_2O/Cl^-) [f]	0.78 ± 0.01		2.20 ± 0.01	

[a] Charges are omitted for simplicity. M denotes RhCp*. Hydrolysis products of the organometallic fragment: logβ [M_2H_{-2}] = −11.12, logβ [M_2H_{-3}] = −19.01 at I = 0.20 M (KCl) and logβ [M_2H_{-2}] = −8.53, logβ [M_2H_{-3}] = −14.26 at I = 0.20 M (KNO_3) taken from Ref. [21]. [b] Z = H_2O or Cl^- for chloride-containing samples; Z = H_2O for chloride-free media. [c] Determined by UV-Vis spectrophotometry at pH 0.7-2. [d] As H^+ is defined as a component, H_{-1} indicates the deprotonation of a coordinated H_2O molecule, or coordination of OH^-. [e] log K* = log β [MLZ] − pK (HL). [f] For the $[RhCp^*(L)(H_2O)]^+ + Cl^- \rightleftharpoons [RhCp^*(L)Cl] + H_2O$ equilibrium determined at various total chloride concentrations by UV-Vis.

Table 3

In vitro cytotoxicity (IC_{50} values in μM) of the RhCp* complexes of dhp (**1**), pic (**2**) and maltol for comparison[a]

Cell line	1	2	maltolato complex[b]
CH1	50 ± 2	258 ± 6	120 ± 16
SW480	112 ± 15	283 ± 65	178 ± 26
A549	165 ± 14	343 ± 24	306 ± 34

[a] 96 h exposure, [b] Data taken from Ref. [21]